Solar Phys (2012) 281:391–409
DOI 10.1007/s11207-012-9957-0

THE SUN 360

Observations of ICMEs and ICME-like Solar Wind Structures from 2007 – 2010 Using Near-Earth and STEREO Observations

E.K.J. Kilpua · L.K. Jian · Y. Li · J.G. Luhmann · C.T. Russell

Received: 14 October 2011 / Accepted: 13 February 2012 / Published online: 28 March 2012

Abstract The generally low interplanetary magnetic field magnitude around the minimum between Solar Cycles 23 and 24 (SC 23/24 minimum) allows us to identify weak and small solar wind structures. We use observations from near-Earth and twin STEREO spacecraft to study solar wind conditions from January 2007 through December 2010. In addition to 84 clear interplanetary coronal mass ejections (ICMEs), we identified 58 ICME-like transients, which exhibit some classical ICME signatures but have weak magnetic fields ($<$ 7 nT) and/or short durations ($<$ 10 hours). The number of ICME-like transients peaked during the SC 23/24 minimum, while the ICME rate increased with increasing solar activity. The magnetic structures of flux rope type ICMEs and transients show similar solar cycle variation trends, suggesting that ICMEs and transients originate from similar polarity regions at the Sun. We observed a gradual transition from ICME-like structures to ICMEs. The identified events display continuous distributions in duration and magnetic field magnitude ranging from a few hours to several days and from a few nanoteslas to a few tens of nanoteslas, respectively. Our ICME-like transient rate (less than one event/month) is considerably smaller than that suggested by solar observations of narrow CMEs. This implies that the majority of small coronal ejections are merged as a part of the solar wind by the time they reach 1 AU. We found that ICME-like transients generally occur closer to stream interaction regions (SIRs) than ICMEs, and the majority of the events we identified in declining parts of fast solar wind streams were ICME-like structures. This suggests that ICME-like transients tend to arise close to coronal hole boundaries and thus may have an important role in coro-

The Sun 360
Guest Editors: Bernhard Fleck, Bernd Heber, Angelos Vourlidas

E.K.J. Kilpua (✉)
Department of Physics, Division of Geophysics and Astronomy, University of Helsinki, Helsinki, Finland
e-mail: Emilia.Kilpua@helsinki.fi

E.K.J. Kilpua · L.K. Jian · C.T. Russell
Institute of Geophysics and Planetary Physics, University of California, Los Angeles, CA, USA

Y. Li · J.G. Luhmann
Space Sciences Laboratory, University of California, Berkeley, CA, USA

nal hole dynamics. Diverse solar wind transients presumably manifest the variation of solar eruptions from small-scale blobs to wide CMEs.

Keywords Interplanetary coronal mass ejection · Solar wind · Solar minimum · Interplanetary magnetic field · Coronal mass ejection · Flux rope

1. Introduction

Coronal mass ejections (CMEs) are powerful explosions of solar plasma and magnetic flux. After being released from the Sun, CMEs propagate out into the heliosphere, becoming a part of the solar wind flow. Over the years various interplanetary magnetic field as well as solar wind plasma and compositional signatures have manifested CMEs in the interplanetary medium (see, *e.g.*, Gosling, 1990; Neugebauer and Goldstein, 1997; Zurbuchen and Richardson, 2006). However, despite several decades of intensive research, there is no clear consensus on which solar wind structures are interplanetary manifestations of CMEs (ICMEs). The problem is that no *in situ* signature would be present in all ICMEs, and different signatures may come and go during a given ICME. Also, CMEs may lose their individual characteristics as they travel through the interplanetary medium due to interaction with the ambient solar wind flow or with other CMEs (Burlaga, Plunkett, and St. Cyr, 2002).

Most studies (*e.g.*, Huttunen *et al.*, 2005; Jian *et al.*, 2006; Lepping *et al.*, 2006; Richardson and Cane, 2010; Jian, Russell, and Luhmann, 2011) that catalogue and analyze ICMEs concentrate only on obvious cases; some of them in particular on magnetic clouds (Burlaga *et al.*, 1981), which are a special subset of ICMEs showing enhanced magnetic field magnitudes, low temperatures, and smoothly rotating magnetic field direction. However, a broad spectrum of solar wind transients that exhibit some classical ICME signatures, but are less well defined, have been reported including complex ICMEs and small magnetic flux ropes (Moldwin *et al.*, 2000; Burlaga, Plunkett, and St. Cyr, 2002; Cartwright and Moldwin, 2008; Feng *et al.*, 2008; Kilpua *et al.*, 2009a). It is currently not understood how these "ICME-like structures" and clear ICMEs are related, whether they are manifestations of the same type of solar eruptions or have fundamentally different origins.

Remote white-light observations by the *Solar TErrestrial RElations Observatory* (STEREO; Kaiser *et al.*, 2008) and the *Solar and Heliospheric Observatory* (SOHO) have revealed that CMEs range from powerful CMEs affecting the Sun globally to poorly defined narrow white-light features called narrow CMEs or streamer blobs (Sheeley *et al.*, 1997; Wang *et al.*, 2000; Gilbert *et al.*, 2001; Sheeley *et al.*, 2008). The LASCO CME catalogue reports narrow CMEs several times per day, even during the deepest time of solar minimum. At least part of the narrow CMEs/streamer blobs are consistent with a flux rope topology, as was demonstrated by Sheeley *et al.* (2009) who analyzed their characteristics using nearly simultaneous observations from widely separated STEREO spacecraft. Using the recent observations from white-light heliospheric imagers onboard STEREO, Rouillard *et al.* (2011) followed weak coronal eruptions all the way to the orbit of the Earth, where the associated ICME signatures were identified.

The abundance of narrow CMEs released from the Sun suggests that they may form a significant part of the slow solar wind component. As only a minority of ejections have high enough densities to be followed at large heliospheric distances in white-light observations, it is not clear how weak coronal ejections are generally manifested in the solar wind. It is also possible that most of them are washed out due to plasma interaction processes with the ambient solar wind. Narrow CMEs share several similarities with wide CMEs (Gilbert *et al.*, 2001); thus a natural starting point in seeking their interplanetary counterparts is to search for signatures of small and weak ICME-like structures.

In this paper we investigate ICMEs and ICME-like transients from January 2007 through December 2010. The recent extended and deep solar minimum following Solar Cycle 23 (SC 23/24 minimum) presents an ideal period to distinguish weak and small solar wind structures from the ambient solar wind. As shown by Jian, Russell, and Luhmann (2011), in comparison with the previous three minima, the interplanetary magnetic field (IMF) was about 30 % weaker and the total pressure (sum of magnetic pressure and plasma thermal pressure) was more than 36 % weaker during the SC 23/24 minimum. Also, during most of our study period the near-Earth and STEREO spacecraft have provided continuous solar wind observations from three well-separated vantage points, thus allowing us to gather larger statistics than was possible during previous solar minima. In Section 2 we present our data sets and analysis methods. In Section 3 we analyze and compare the occurrence rate, properties, and magnetic structure of transients and ICMEs. We discuss and summarize our results in Section 4.

2. Data and Approach

Based on the sunspot number levels, we take the period of July 2008 – June 2009 to represent the SC 23/24 minimum (see also the discussion in Jian, Russell, and Luhmann, 2011). We refer to the period from January 2007 to June 2008 as the "late declining phase of SC 23" and the period from July 2009 to December 2010 as the "early rising phase of SC 24" (see also Table 4).

The STEREO data sets used come from the magnetometers (MAG) and solar wind electron analyzers (SWEAs) of the *In-situ Measurements of Particles and CME Transients* (IMPACT) instrument package, and from the *Plasma and Supra-Thermal Ion Composition* (PLASTIC) investigation described in Acuña *et al.* (2008), Sauvaud *et al.* (2008), and Galvin *et al.* (2008), respectively. To monitor solar wind conditions at L1 we use primarily *Wind* observations. From *Wind* we use magnetometer (Lepping *et al.*, 1995) and 3D plasma analyzer (Lin *et al.*, 1995) measurements. The separation between STEREO-A and STEREO-B increased from about zero to almost 180° in the course of this study. A few multi-spacecraft ICME encounters took place mainly in 2007 and are described in Kilpua *et al.* (2011a).

In this study we consider the following ICME signatures, which are summarized and discussed, *e.g.*, by Zurbuchen and Richardson (2006): enhanced magnetic field magnitude, low magnetic field variance, organized magnetic field directional changes, depressed proton temperature, depressed plasma beta, declining solar wind speed and fast forward shocks and intervals of bidirectional suprathermal electrons (BDEs). BDE intervals observed during the ICMEs have been interpreted to imply closed magnetic structures, in which the field lines are attached to the Sun at both ends (see, *e.g.*, Gosling, 1990; Malandraki *et al.*, 2000).

For the event selection we require that at least one of the magnetic field signatures and two other features listed above are present. The event boundaries are determined primarily from the magnetic field signatures. We used magnetic field as our main identification criterion because periods of low temperature and plasma beta, as well as BDEs often occur outside ICMEs too (Richardson and Cane, 1995; Lavraud *et al.*, 2010). We also did not consider plasma compositional signatures (Zurbuchen and Richardson, 2006), such as elevated helium to proton ratio and enhanced iron and oxygen charge states, because the availability of these measurements differs between spacecraft.

In this work we require ICMEs to have maximum magnetic fields (B_{max}) > 7 nT and durations more than ten hours. For ICME-like transients we do not set any threshold value for B_{max}, but we require that they last at least three hours. Our purpose is to investigate separately the ICME population that is included in a "typical" ICME list and smaller and weaker ICME-like structures. 18 % of our ICME-like transients are included in the UCLA STEREO and *Wind*/ACE ICME lists, and only one event is included in the ICME list by Richardson and Cane (2010).

We identified in total 84 ICMEs and 58 ICME-like transients from the STEREO-A, STEREO-B, and L1 spacecraft combined during our four-year study period, as listed in Tables 1, 2, and 3.

We divided our events into three different categories depending on the surrounding solar wind structure. **Category 1** events are surrounded by slow ($< 500\ \mathrm{km\,s^{-1}}$) speed solar wind for at least one day before and after the event interval. **Category 2** events occur close to or within stream interaction regions (SIRs). **Category 3** events are embedded within declining parts of fast solar wind streams.

Next we will present a typical event from each category. For each category we selected an ICME-like transient, as examples of clear ICMEs are represented in several other studies (for examples of ICMEs during our study period, see, *e.g.*, Kilpua *et al.*, 2009b, 2009c, 2011a, and Jian, Russell, and Luhmann, 2011).

Figure 1 shows an example of a Category 1 event that was detected between 16 November 2008 20:45 – 17 November 2008 13:30 UT, 2008 at STEREO-B. It is seen from Figure 1(c) that the event was surrounded by slow solar wind. This ICME-like transient lasted 16.8 hours, but the maximum magnetic field magnitude was only 6.2 nT, thus not much stronger than in normal non-ICME solar wind. Panel (f) shows the total pressure (Pt; sum of the magnetic pressure and plasma thermal pressure) perpendicular to the magnetic field (Russell, Shinde, and Jian, 2005). The Pt profile peaked shortly after the center of the event, which according to Jian *et al.* (2006) signifies that STEREO-B traversed close to the center of this structure. During the indicated event interval the magnetic field variance was low and temperature and plasma beta were slightly depressed with respect to the ambient value. A flat speed profile indicates that this structure did not expand as it passed STEREO-B; the event rather seems to flow along with the ambient solar wind. The pitch angle spectrogram of supra-thermal electrons shows that the heat flux flow was unidirectional during the event, suggesting that magnetic field lines may have reconnected with an open field line from the other end (see, *e.g.*, Baker *et al.*, 2009).

An example of a Category 2 event that was detected between 6 March 2008, 12:15 UT – 6 March 2008, 17:00 UT at STEREO-B is shown in Figure 2. Figure 2(c) shows that the solar wind speed increases abruptly to almost $700\ \mathrm{km\,s^{-1}}$ just after the trailing edge of this ICME-like transient. Presumably, partly due to the compression by the upcoming fast wind, this event had a very high magnetic field magnitude (B_{max} was 16.5 nT), but it lasted only about five hours. During the selected event interval the magnetic field variance was low, and there was a clear drop in plasma beta and a slight depression in temperature. Pt maximized at the stream interface. Pt in the ICME interval shows an increasing trend because of the compression by the following fast stream. Supra-thermal electrons again show a unidirectional flow.

Figure 3 displays an event that was embedded within a declining part of a fast solar wind stream. This ICME-like transient was observed between 2 February 2007, 04:10 UT – 2 February 2007, 14:35 UT at *Wind*. The maximum magnetic field during the event was only 3.7 nT and it lasted about 10 hours. Despite the very low magnetic field magnitude, the structure stood out from the ambient solar wind: The magnetic field variance was low and the temperature and plasma beta were depressed with respect to the ambient values. This event was associated with a bidirectional electron flow (Figure 3(g)), implying a magnetically closed structure.

Table 1 ICMEs and transients identified in the near-Earth solar wind during January 2007 – December 2010. Columns give: Shock time (UT), event start time (UT), event end time (UT); maximum magnetic field magnitude ($B_{\max}$), average solar wind speed (V_{ave}), and duration (ΔT) for each ICME/transient, rotation of the north-south magnetic field component, and the ambient solar wind category (see Section 2 for definition). "nc" signifies that the rotation of the north-south magnetic field was not clear or that we could not place the event in any of our solar wind categories. Times are given in month/day hhmm format.

Shock (UT)	ICME start (UT)	ICME stop (UT)	$B_{\max}$ (nT)	V_{ave} (km s^{-1})	ΔT_{ICME} (hours)	B_Z/B_n type	SW
2007							
–	1/14 1145	1/15 0745	15.2	358	20.0	NS	2
–	1/15 2050	1/16 0445	10.1	518	7.8	NS	2
–	2/2 0410	2/2 1435	3.7	514	18.8	nc	3
–	3/24 0515	3/24 1230	10.9	364	7.3	nc	2
–	3/29 1505	3/30 0020	6.2	396	9.2	N	3
–	5/21 2245	5/22 1555	14.8	445	19.2	N	nc
–	6/8 0545	6/9 0515	9.6	362	23.5	nc	2
–	7/23 2100	7/24 0945	3.2	377	12.8	nc	3
11/19 1722	11/20 0025	11/20 1150	14.6	462	0.13	NS	2
–	12/25 1515	12/26 0810	6.2	354	12.4	NS	3
2008							
–	3/8 1745	3/9 0440	14.5	452	11.4	NS	2
–	5/23 0120	5/23 1050	5.2	408	9.1	NS	3
–	7/25 1325	7/25 2330	5.2	408	10.1	NS	3
–	7/31 1150	7/31 1530	7.1	380	3.7	N	1
–	9/3 1630	9/4 0345	13.5	461	11.3	NS	2
9/16 1233	9/17 0400	9/18 0805	7.2	410	28.1	1	
–	10/8 0445	10/8 2015	5.5	353	15.5	nc	3
–	11/1 0730	11/1 1530	5.3	491	8.0	nc	3
–	12/4 1125	12/5 1110	7.3	386	23.8	nc	2
–	12/5 1745	12/05 2200	11.0	430	4.3	NS	2
–	12/17 0330	12/17 1530	9.8	343	12.0	NS	1
2009							
–	1/19 0125	1/19 0510	13.4	430	3.8	nc	2
–	1/26 0500	1/26 1520	11.1	380	10.3	nc	1
2/3 1921	2/4 0250	2/4 1845	11.2	355	15.2	NS	1
3/11 2201	3/12 0120	3/13 0145	18.6	365	24.4	N	2
–	4/5 1700	4/6 0745	3.6	344	14.8	nc	1
–	4/22 1415	4/22 2045	4.4	390	6.0	NS	3
6/27 1104	6/27 1805	6/28 2030	12.2	390	26.6	NS	3
–	7/21 0215	7/22 0440	14.5	321	25.9	NS	2
–	8/5 1215	8/6 0555	14.6	325	17.2	N	2
–	8/7 1220	8/7 1640	6.6	375	4.2	N	2
8/30 0018	8/30 0835	8/30 1445	12.7	401	6.3	nc	2
–	9/30 0705	9/30 1925	9.3	347	12.3	N	2

Table 1 (*Continued*)

Shock (UT)	ICME start (UT)	ICME stop (UT)	B_{max} (nT)	V_{ave} (km s^{-1})	ΔT_{ICME} (hours)	B_Z/B_n type	SW
–	10/12 1300	10/12 2150	6.8	347	8.8	N	1
–	10/17 1730	10/18 1340	3.7	316	20.2	NS	3
–	10/29 0130	10/29 2340	11.3	362	22.2	NS	3
–	11/14 1055	11/15 1150	8.4	335	24.9	nc	1
–	11/20 1840	11/21 0205	11.3	415	5.4	NS	1
12/12 0439	12/12 1925	12/13 2345	8.2	271	28.2	NS	1
2010							
–	1/1 2310	1/3 1320	8.8	287	13.2	NS	1
2/7 1810	2/8 0000	2/9 0730	10.7	355	7.5	N	1
4/5 0835	4/5 1240	4/6 1400	19.1	643	26.7	nc	nc
4/11 1315	4/11 2130	4/12 1620	12.1	412	18.8	nc	1
–	5/18 0420	5/19 1005	11.5	355	19.8	SN	1
5/28 0245	5/28 1810	5/29 1755	15.0	355	23.8	S	1
–	6/21 0720	6/22 1625	7.3	359	33.1	N	1
8/3 1810	8/4 0450	8/4 1035	18.1	567	5.8	N	nc
–	8/4 1125	8/5 0135	14.0	539	14.2	NS	nc
–	9/25 1440	9/26 0940	3.8	469	19.2	nc	nc
–	10/11 0550	10/11 1830	14.4	355	12.7	nc	3
12/19 2030	12/19 2255	12/20 2250	10.0	385	23.9	nc	2

3. Observations

3.1. Event Occurrence Rate

Figure 4 compares the sunspot number and the CME rate with the number of ICMEs and ICME-like structures identified during our study period. Panel (a) shows the monthly (blue) and monthly smoothed (red) sunspot numbers from the Solar Influences Data Center (SIDC). The next panels show the monthly CME rate. We show separately from the online LASCO CME catalogue the events that have angular widths (AW) larger and smaller than 30°. This division is made because over the years the identification criteria has been changed to include smaller events in the LASCO CME catalogue to get a better agreement with the automated CACTUS catalogue (Yashiro, Michalek, and Gopalswamy, 2008). We also expect that wider CMEs are associated with ICMEs, while narrower CMEs might be the sources of our ICME-like transients. Panel (d) shows the tilt angle of the heliospheric current sheet (HCS) computed by Wilcox Solar Observatory. Panels (e) and (f) show the monthly number of ICMEs and transients, respectively, combined from the near-Earth, STEREO-A, and STEREO-B, observations.

Table 4 gives the number of ICMEs and ICME-like transients as well as the number of events in each solar wind category (see Section 2) during the late declining phase of SC 23, the SC 23/24 minimum, and the early rising phase of SC 24. Since our SC 23/24 minimum period lasts 12 months, while the other two periods last 18 months, we have multiplied the values during the SC 23/24 minimum by 1.5 to allow direct comparison.

Table 2 ICMEs identified by STEREO-A during 2007 – 2010. Columns are same as in Table 1.

Shock (UT)	ICME start (UT)	ICME stop (UT)	B_{max} (nT)	V_{ave} (km s^{-1})	ΔT_{ICME} (hours)	B_Z/B_n type	SW
2007							
–	1/14 1240	1/15 0725	14.7	nd	18.8	NS	nd
–	1/15 2210	1/16 0340	8.6	nd	5.5	NS	nd
–	3/24 0245	3/24 0930	12.1	363	6.9	nc	2
–	3/29 1305	3/29 2040	5.9	407	7.6	N	3
–	7/20 1300	7/21 0120	11.9	326	12.3	nx	2
8/25 2029	8/25 2345	8/26 1615	15.7	363	16.5	SN	2
–	11/19 2205	11/21 0205	17.6	441	28.0	NS	2
–	12/25 2230	12/26 0630	5.3	428	8.0	nc	3
2008							
–	3/21 0805	3/21 1745	8.5	485	9.7	S	3
nd	5/11 1100	5/12 0555	14.5	nd	17.9	N	1
7/5 0045	7/5 0640	7/6 1815	10.1	333	35.6	N	1
–	9/4 1315	9/5 1215	10.1	325	23.0	N	1
–	10/14 1845	10/15 1345	8.3	421	19.0	N	1
10/31 0324	10/31 1200	10/31 1630	16.2	362	4.5	N	2
–	11/7 0200	11/8 0115	7.1	344	23.3	NS	2
–	11/28 0745	11/28 1825	7.8	287	10.5	N	2
2009							
–	1/21 1430	1/22 0640	5.2	397	16.2	nc	1
–	1/25 1830	1/27 0940	12.4	375	39.2	nc	1
–	2/21 0955	2/21 1530	6.5	387	5.4	NS	3
–	3/4 0050	3/4 0820	11.0	381	7.5	NS	1
–	4/26 0815	4/27 0005	4.5	313	15.8	nc	1
–	4/30 1110	4/30 1730	10.6	298	16.3	NS	1
–	4/30 2030	5/1 0925	8.6	311	12.9	nc	1
–	6/3 0030	6/5 0240	11.2	453	50.2	NS	3
–	7/11 2255	7/13 0550	9.5	334	30.9	NS	2
–	9/8 1025	9/8 1640	14.5	371	30.1	nc	2
–	10/3 0240	10/3 1720	4.9	397	14.7		3
10/16 1456	10/16 2130	10/18 0105	10.8	327	27.6	NS	1
–	10/30 0115	10/30 1620	6.2	388	15.1	nc	1
–	11/1 0150	11/3 0310	8.9	533	49.3	S	1
–	11/14 1830	11/15 1930	9.3	306	25.0	nc	1
–	11/27 0420	11/27 2025	6.9	336	16.1	NS	1
12/8 2338	12/9 0840	12/10 0230	12.1	327	17.8	NS	1

It is seen from Figure 4 and Table 4 that the number of ICME-like transients peaks during the SC 23/24 minimum, while the number of ICMEs increases with increasing solar activity. The number of events reported for the late declining phase of SC 23 might be underestimated, as the probability of detecting separate ICMEs is expected to increase when

Table 2 (*Continued*)

Shock (UT)	ICME start (UT)	ICME stop (UT)	B_{max} (nT)	V_{ave} (km s^{-1})	ΔT_{ICME} (hours)	B_Z/B_n type	SW
2010							
–	2/4 1050	2/4 1845	6.1	364	7.9	nc	1
2/5 0333	2/5 1230	2/6 0230	13.9	402	14.0	NS	2
–	3/5 1735	3/6 0930	12.5	357	15.9	nc	1
5/30 1457	5/31 0025	5/31 1630	9.7	409	16.1	NS	1
6/3 0836	6/3 1220	6/4 1640	17.8	364	28.3	nc	2
–	6/16 1510	6/18 0340	8.8	450	36.5	N	3
–	8/18 0740	8/19 0610	7.0	336	22.5	NS	1
8/20 1613	8/20 2220	8/22 0310	18.3	562	28.8	nc	1
–	8/31 0140	8/31 1020	18.3	463	8.7	nc	2
9/11 0658	9/11 1710	9/13 1030	16.9	468	41.3	S	1
–	9/16 1550	9/17 0350	6.9	358	12.0	nc	1
9/17 2233	9/18 0620	9/19 0720	16.1	391	25.0	S	1
–	12/14 0940	12/14 1335	11.8	398	3.9	N	1
12/14 1715	12/15 0850	12/16 0535	19.9	482	20.4	NS	2

the STEREO spacecraft drift farther away from the Earth. The number of wide CMEs almost tripled from the SC 23/24 minimum to the early rising phase of SC 24. However, as shown by Table 4, there was only a slight increase in the ICME rate between these two periods. In this study *in situ* events were identified from the near-ecliptic solar wind observations, while Figures 4(b) and (c) include CMEs launched to all latitudes. An abrupt increase in the HCS in late 2009 (Figure 4(d)) suggests that at that time the coronal streamer belt neutral line and consequently the source regions of CMEs were shifted to higher latitudes. The narrow CME rate decreased strongly from the maximum of more than 120 events per month in April 2007 to only a few tens of events per month by the SC 23/24 minimum. The number of narrow CMEs remained low during the early rising phase of SC 24.

Table 4 reveals that during the late declining phase of SC 23 the majority of events were associated with SIRs or occurred within declining parts of fast solar wind streams. Only two (8 %) events were surrounded by slow solar wind flow. The fraction of slow solar wind events increased considerably during the SC 23/24 minimum, and during the early rising phase of SC 24 about half (51 %) of the events were embedded within the slow solar wind. The average magnetic field magnitudes as well as the durations for ICMEs and ICME-like transients increased when the solar activity increased during the early rising phase of SC 24.

3.2. ICME/Transient Properties

The division of our events into three ambient solar wind categories (see Section 2) is shown in Table 5. ICME-like transients were evenly divided into the three categories, while the majority of ICMEs were identified as either embedded in slow solar wind (49 %) or close to SIRs (45 %). Only five ICMEs (6 %) were detected within declining parts of fast solar wind.

The scatter plot of maximum magnetic field and duration is shown in Figure 5. The pair of black vertical lines bounds the event interval. Different colors indicate different solar wind categories (see the figure caption). The horizontal and vertical lines indicate the

Table 3 ICMEs identified by STEREO-B during 2007 – 2010. Columns are same as in Table 1.

Shock (UT)	ICME start (UT)	ICME stop (UT)	B_{max} (nT)	V_{ave} (km s^{-1})	ΔT_{ICME} (hours)	B_Z/B_n type	SW
2007							
nd	1/14 1245	1/15 0820	14.6	nd	17.6	NS	nd
nd	1/15 2125	1/16 0330	9.8	nd	5.9	NS	nd
–	3/24 0435	3/24 1720	11.8	376	12.9	nc	2
–	5/22 0435	5/22 2150	17.5	460	17.4	N	nc
–	6/8 0540	6/9 0810	11.1	371	26.5	nc	2
–	6/28 1635	6/29 0905	7.3	399	16.7	nc	2
–	10/23 1645	10/23 2345	10.3	377	7.0	n	2
11/19 1349	11/19 2255	11/20 0905	16.9	464	10.2	nc	2
–	12/30 0615	1/1 0230	11.9	314	44.3	NS	1
2008							
–	2/5 2050	2/7 1130	13.0	375	14.7	SN	2
–	3/6 1215	3/6 1700	16.5	430	4.8	nc	2
4/29 1410	4/29 1420	4/29 2050	12.5	449	6.2	N	2
–	5/15 2155	5/16/1755	3.8	457	20.0	nc	3
–	6/3 1220	6/3 1620	3.2	483	4.0	NS	3
6/6 1535	6/6 2200	6/7 1215	14.9	413	14.3	NS	1
–	7/6 0155	7/6 1325	3.1	291	11.5	nc	1
–	7/10 2245	7/11 0730	11.9	562	8.8	NS	2
–	8/14 0455	8/15 0145	5.7	363	20.8	nc	1
–	8/15 1130	8/16 0100	9.4	351	13.5	NS	2
–	9/28 0230	9/28 1400	9.3	368	11.5	nc	2
–	10/17 1000	10/18 0545	8.0	317	17.8	SN	1
–	10/19 0130	10/20 1140	9.5	347	34.2	NS	2
–	11/16 2045	11/17 1330	6.2	314	16.9	nc	1
12/7 0435	12/7 1550	12/8 1145	8.7	316	19.9	nc	2
–	12/8 1700	12/8 2030	18.2	340	3.5	NS	2
–	12/18 1615	12/18 2255	7.5	370	6.7	nc	2
–	12/31 0200	1/1 0135	9.5	403	23.6	NS	3
2009							
–	1/13 0400	1/13 2145	11.2	320	17.8	NS	2
–	1/27 0535	1/27 1040	9.0	401	5.1	NS	2
3/14 0946	3/14 2000	3/15 1645	10.3	386	20.8	SN	1
–	6/08 2330	6/10 1620	2.8	317	40.8	nc	3
6/19 0023	6/19 0800	6/20 2130	11.1	306	37.5	NS	1
–	7/16 1250	7/17 1900	9.4	310	30.2	NS	2
–	7/31 0310	7/31 1915	10.0	390	16.1	NS	1
–	8/6 0420	8/7 0500	13.6	413	25.7	NS	2
–	8/25 0910	8/26 1400	10.8	330	28.8	NS	1
–	8/30 1730	8/31 0830	11.9	359	15.0	nc	2
–	9/10 0250	9/11 0720	8.5	307	28.5	N	2

Table 3 (*Continued*)

Shock (UT)	ICME start (UT)	ICME stop (UT)	B_{max} (nT)	V_{ave} (km s^{-1})	ΔT_{ICME} (hours)	B_Z/B_n type	SW
–	10/2 2010	10/4 0650	13.1	322	34.8	S	1
–	11/4 2000	11/05 0110	5.5	417	5.2	N	3
–	11/10 1900	11/11 1840	11.4	355	23.7	NS	1
–	11/19 1810	11/20 1430	4.8	377	20.3	nc	3
–	11/27 1235	11/27 2115	10.3	337	10.8	nc	2
–	12/29 1925	12/30 0930	12.0	325	14.1	NS	1
2010							
–	1/20 1955	1/21 2220	7.1	318	26.4	NS	1
–	3/1 2315	3/2 0700	15.0	356	7.8	NS	2
–	4/13 2155	4/14 0815	13.8	413	10.3	nc	1
6/7 0408	6/7 2205	6/8 1345	11.5	369	15.8	SN	1
–	6/15 0320	6/16 1620	5.7	396	37.0	SN	3
–	6/23 2310	6/24/2150	7.9	442	22.8	SN	2
–	7/15 2120	7/16 1410	5.3	341	16.8	nc	1
–	7/22 0135	7/22 1840	8.5	433	17.3	nc	2
8/2 1531	8/3 0455	8/3 1010	32.2	636	5.2	S	nc
–	8/3 1425	8/4 0725	13.1	593	17.0	nc	nc
9/15 2320	9/16 1050	9/17 0735	12.4	387	11.2	nc	2
–	9/19 2010	9/20 0630	5.7	492	10.3	S	nc
–	10/30 1815	10/31 0715	10.1	374	13.0	nc	1
11/7 1905	11/8 0200	11/9 0910	17.5	397	31.2	NS	2
11/19 2026	11/20 0630	11/21 0850	11.8	386	26.3	SN	2
–	12/2 0930	12/3 1200	7.4	344	26.5	nc	2
–	12/17 0140	12/18 2040	10.0	347	43.0	NS	1
–	12/25 2020	12/27 0640	11.6	306	34.3	NS	1

threshold values for B_{max} (7 nT) and duration (ten hours) that were used to divide between ICMEs and ICME-like transients. ICMEs are located in the upper right portion of Figure 5. It is evident from the scatter plot that ICME-like transients are grouped depending on the surrounding solar wind speed structure. ICME-like transients that have maximum magnetic fields above 7 nT, but durations below ten hours were located close to or within SIRs (upper left portion), while transients with durations longer than ten hours, but magnetic fields below 7 nT were either embedded within slow solar wind or occurred within declining parts of fast wind (lower right portion). The majority of events associated with both low magnetic field magnitudes and short durations were found within declining parts of fast solar wind (lower left portion).

Average B_{max}, V_{ave}, and duration for ICMEs and ICME-like structures in each solar wind category are also shown in Table 6. The average speeds are similar for ICMEs and ICME-like structures, except for the events associated with SIRs. As shown in Figure 5, SIR-related ICME-like structures had low durations, but they had speeds 10 % faster and magnetic fields 16 % greater than SIR-related ICMEs. For the other two categories, ICME-like structures had clearly lower magnetic fields than ICMEs. From Table 6 it is seen that SIR and slow solar wind related ICMEs have remarkably similar magnetic field magnitudes, durations,

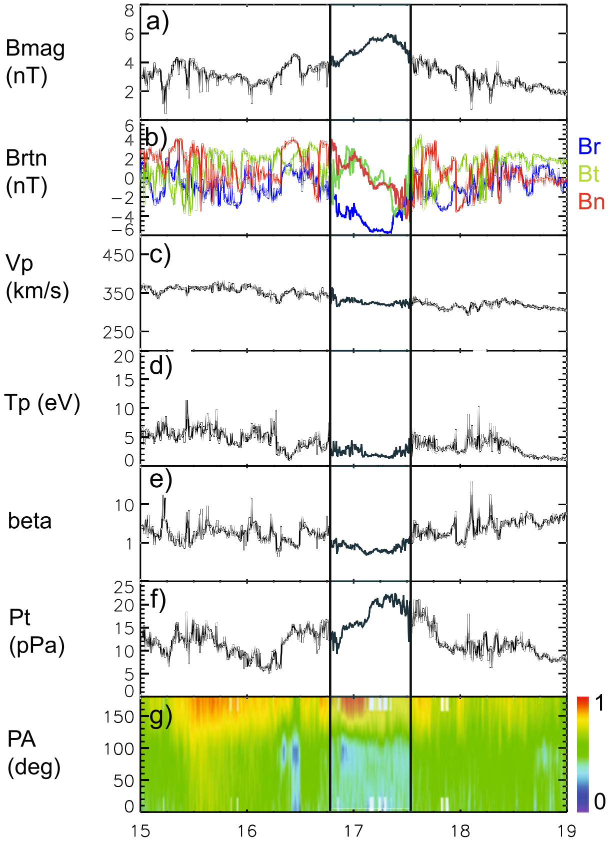

Figure 1 Example of an ICME-like transient surrounded by slow speed solar wind identified by STEREO-B between 16 November 2008, 20:45 UT – 17 November 2008, 13:30 UT. Panels show: (a) magnetic field magnitude, (b) magnetic field components in RTN coordinates (blue: B_R, green: B_T, red: B_N), (c) solar wind speed, (d) solar wind proton temperature, (e) proton beta, (f) total perpendicular pressure, and (g) supra-thermal electron pitch angle spectrogram of 246 eV electrons. The color coding indicates the relative amplitude of the distribution functions, running from blue (lowest values) to red (highest values). The pair of black vertical lines bounds the event interval.

and average speeds. ICMEs detected in declining parts of fast solar wind had lower magnetic fields and longer durations than the ICMEs in the other two categories.

Tables 1 – 3 also indicate whether ICMEs or ICME-like structures drove a fast forward shock. About one third of ICMEs (34 %) were associated with a leading shock, while only 13 % of ICME-like structures drove a shock. As discussed above, the average speeds were similar for ICMEs and ICME-like structures. However, a considerably larger fraction of ICME-like structures than ICMEs (6 % and 34 % respectively) were embedded in the declining portion of fast streams, implying that more ICME-like structures were preceded by high-speed solar wind and thus could not generate leading forward shocks.

The distributions shown in Figure 6 demonstrate that events were observed in a continuous manner from a few nanoteslas to a few tens of nanoteslas and from three hours to more than two days. The number of events increases sharply when the magnetic field increases over 4 nT. Only six events with $B_{max} < 4$ nT have been included in our data set. The number of events peaks in the 10 – 12 nT bin, and there is a sharp drop in event counts for $B_{max} > 12$ nT. 71 % of identified events had B_{max} below 12 nT. The duration distribution peaks in the three–eight hours bin, and the number of events decreases rather monotonously with increasing duration after reaching the 13 – 18 hour bin.

We also analyzed the magnetic structure of our events. We refer to events as flux ropes if they show coherent rotation of the magnetic field. We classified flux rope events according to the behavior of the north-south magnetic field components: for *bipolar* flux ropes the

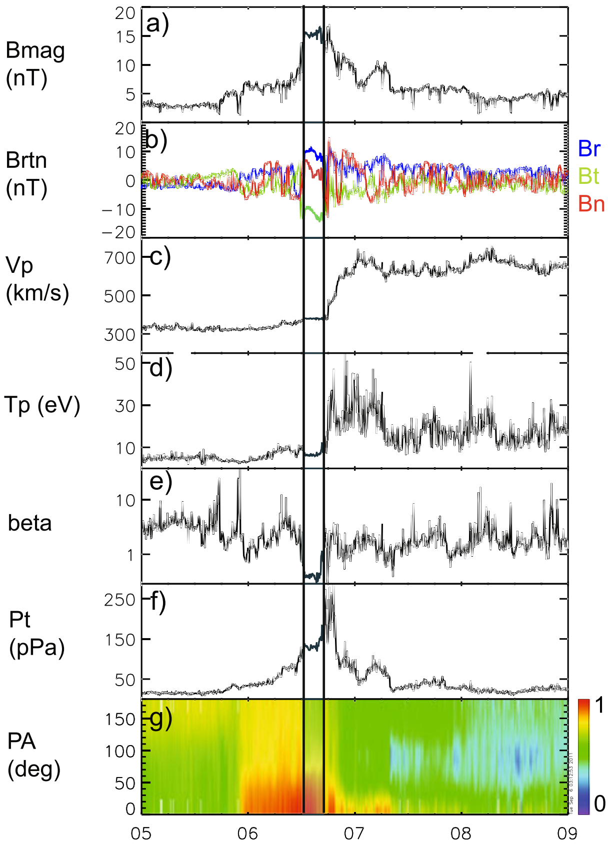

Figure 2 Example of an ICME-like transient detected within a SIR between 6 March 2008, 12:15 UT – 6 March 2008 17:00 UT at STEREO-B. Panels are same as in Figure 1.

north-south component changes its sign, and for *unipolar* flux ropes the north-south component maintains its sign during the passage of the flux rope (Bothmer and Schwenn, 1998; Mulligan, Russell, and Luhmann, 1998). The division of flux ropes into unipolar and bipolar classifications reflects the tilt of the flux rope axis with respect to the ecliptic plane. Bipolar flux ropes have low inclination, while unipolar flux ropes are oriented roughly perpendicular to the ecliptic plane. We further divide bipolar events into SN- and NS-types, depending on whether the north-south component rotates from south to north or from north to south, respectively. Similarly, unipolar flux ropes are divided into S- and N-type events. Table 5 shows the division of ICMEs and ICME-like transients into different flux rope types. 76 % of ICMEs were flux ropes, while only 45 % of ICME-like transients showed coherent magnetic field rotation. Due to generally low magnetic fields, it is probably difficult to define the rotation for ICME-like structures. Distributions of ICMEs and ICME-like transients to unipolar and bipolar flux ropes, as well as to different flux rope types are rather similar. For event classes, bipolar flux ropes dominate unipolar, and for bipolar flux ropes considerably more events with north-south rotations are observed. For ICMEs the fraction of SN-type flux ropes was larger (13 %) than for ICME-like transients, for which only one event was associated with a south-to-north rotating magnetic field.

Further, from Table 5 the fraction of flux rope type events from all events increased from 57 % during the late declining phase of SC 23 to almost 70 % for the rest of our study period. Five out of the total of nine SN-type events occurred during the early rising phase of SC 24.

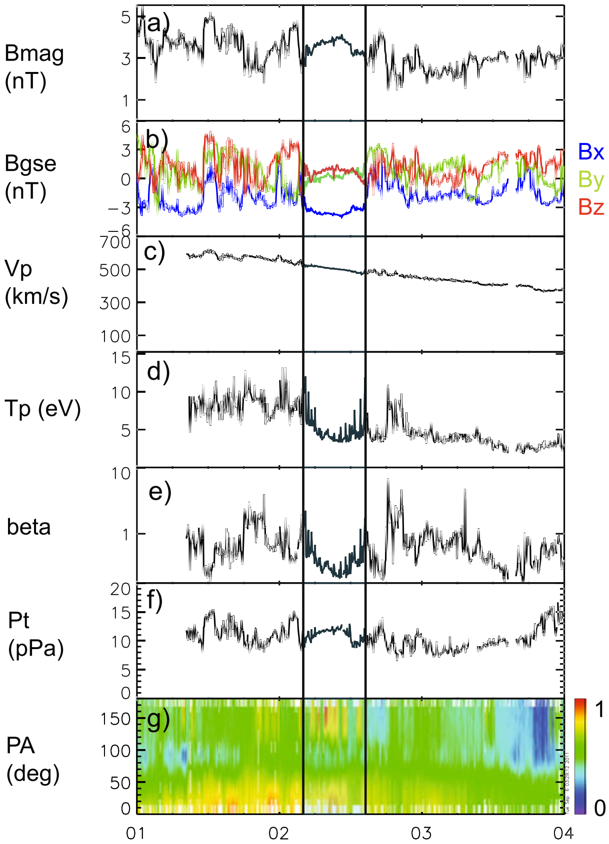

Figure 3 Example of an ICME-like transient detected within declining part of a fast solar wind stream that was identified by the near-Earth spacecraft (data shown from *Wind*) between 2 February 2007, 04:10 UT – 2 February 2007, 14:35 UT. Panels show: (a) magnetic field magnitude, (b) magnetic field components in GSE coordinates (blue: B_X, green: B_Y, red: B_Z), (c) solar wind speed, (d) solar wind proton temperature, (e) proton beta, (f) total perpendicular pressure, and (g) supra-thermal electron pitch angle spectrogram of 260 eV electrons. The color coding indicates the relative amplitude of the distribution functions, running from blue (lowest values) to red (highest values). The pair of black vertical lines bounds the event interval.

4. Discussion and Summary

In this paper we have studied properties of ICMEs and ICME-like transients using observations from near-Earth and STEREO spacecraft from January 2007 through December 2010. We defined ICME-like transients as events showing some classical ICME signatures and with magnetic field less than 7 nT and/or duration shorter than ten hours; hence, in our study ICMEs have maximum magnetic fields above 7 nT and durations longer than ten hours.

We identified ICME-like structures continuously, from short and weak events to large-scale ICMEs with high magnetic field magnitudes. A sharp drop in the event counts occurred at a magnetic field of 12 nT and a duration of 18 hours, thus at considerably higher values than the threshold values we used to distinguish between ICMEs and ICME-like transients (7 nT and 10 hours respectively). We expect that these drops reflect the lack of strong CMEs at solar minimum. It has been shown that ICMEs tend to be weaker and smaller at solar minimum than near solar maximum (see, *e.g.*, Jian *et al.*, 2006).

Our statistics showed that during the early rising phase of Cycle 24, when the sunspot activity and the CME rate clearly increased, there was only a modest increase in the near-ecliptic ICME rate. As discussed in Section 3.1 and by Kilpua *et al.* (2011b), this likely results from the shift of the CME source regions to higher latitudes. The decline in the number of ICME-like transients with increasing solar activity could be explained by their identification becoming more difficult due to more complex ambient solar wind background

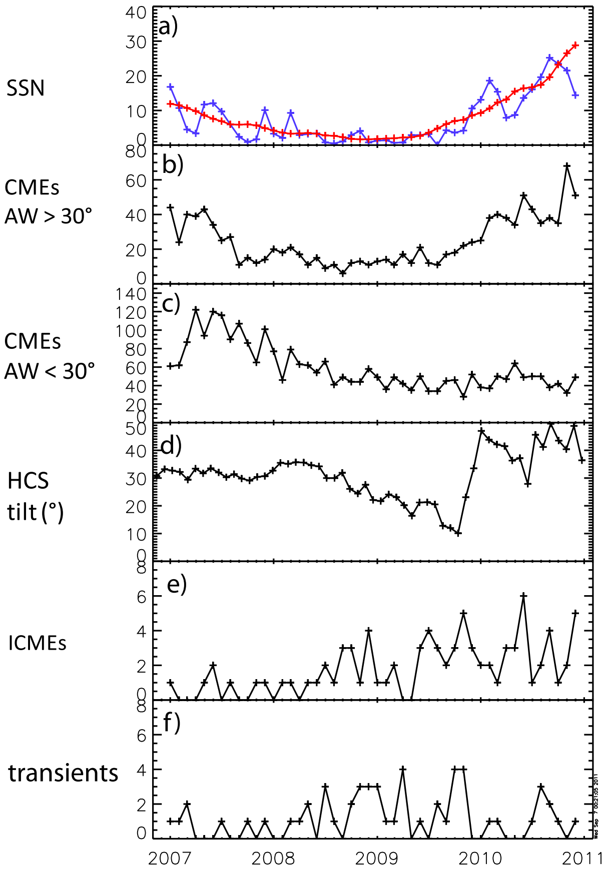

Figure 4 Solar activity and ICME rate during 2007 – 2010. Panels show: (a) monthly (blue) and monthly smoothed (red) sunspot number from SIDC, the monthly rate of CMEs with angular width (AW) (b) > 30° and (c) < 30° from the LASCO CME catalogue, (d) tilt angle of the HCS computed by Wilcox Solar Observatory, and the monthly rate of (e) ICMEs and (f) ICME-like structures from L1, STEREO-A, and STEREO-B combined.

and to CMEs generally increasing in strength (Vourlidas *et al.*, 2011). In our study the number of narrow CMEs and the ICME-like transient rate did not correlate. However, this could be simply explained by difficulties in identifying most *in situ* counterparts for narrow CMEs. The link between narrow CMEs and small *in situ* transients was established by Rouillard *et al.* (2011), who showed that five of the six ICME-like transients they analyzed were associated with poor white-light features. One event was associated with a major CME eruption that was encountered far away from the center.

ICMEs and ICME-like structures were divided similarly into different flux rope types. This similar division suggests that ICMEs and ICME-like structures originate from solar source regions having similar magnetic polarities. Note also that, during the recent unusually deep and extended solar minimum, flux rope events obeyed the solar cycle dependence confirmed for three previous minima (Bothmer and Schwenn, 1998; Mulligan, Russell, and Luhmann, 1998; Li *et al.*, 2011): NS-type events dominated over SN-type events during most of our study period, and the number of opposite polarity events (SN-type flux ropes) increased during the early rising phase of Cycle 24.

It is instructive to identify and analyze ICME-like transients in order to appreciate the complexity and diversity of the ecliptic solar wind. *In situ* measurements reflect the same variety of transient structures as is visible in white-light remote CME observations. However, it is extremely difficult to show whether there are two (or even more) distinct

Table 4 Number of ICMEs and transients, number of events (ICMEs and transients combined) in three solar wind categories (see Section 2 for definition), average maximum magnetic fields, average speeds and durations for ICMEs/transients and the number of flux rope type events, as well as the number of flux ropes with south-to-north (SN) and north-to-south (NS) rotation during our three study periods. To allow direct comparison, values for the SC 23/24 minimum have been multiplied by 1.5.

	Late declining phase of SC 23	SC 23/24 minimum	Early rising phase of SC 24
Period	Jan. 2007 – June 2008	July 2008 – June 2009	July 2009 – Dec. 2010
ICMEs	11	38	50
Transients	15	32	21
Category 1	2	28	36
Category 2	14	27	27
Category 3	9	15	7
B_{max} (nT)	12.8/8.3	10.3/8.1	11.6/9.8
V_{ave} (km s^{-1})	399.3/431.5	372.2/373.3	370.8/396.8
Δ_{T} (h)	19.8/9.4	22.4/10.9	25.9/13.1
Flux ropes	14 (54 %)	48 (69 %)	48 (68 %)
SN-type	2	2	5
NS-type	7	21	27

Table 5 Division of transients and ICMEs into three solar wind categories (see Section 2) and into different flux rope types. Percentages for different flux rope types are calculated from the total number of events that are flux ropes.

	ICME	Transients	Total
Total number	85	58	140
Category 1	41 (48 %)	17 (30 %)	58 (41 %)
Category 2	39 (46 %)	21 (36 %)	58 (41 %)
Category 3	5 (6 %)	20 (34 %)	24 (18 %)
Flux ropes	64 (76 %)	27 (47 %)	88 (64 %)
Unipolar	19 (30 %)	7 (26 %)	26 (30 %)
Bipolar	45 (70 %)	20 (74 %)	62 (70 %)
SN-type	8 (13 %)	1 (4 %)	9 (10 %)
NS-type	37 (58 %)	19 (70 %)	53 (60 %)
N-type	13 (20 %)	6 (22 %)	19 (22 %)
S-type	6 (9 %)	1 (4 %)	7 (8 %)

classes of events having fundamentally different origins. While Gilbert *et al.* (2001) did not find obvious differences between narrow and wide CMEs, an analysis by Rouillard *et al.* (2011) suggests that they might originate from different heights in the solar atmosphere.

Our analysis of background solar wind also suggests that ICMEs and ICME-like transients originate (at least partly) from different solar regions. ICME-like transients that were associated with SIRs had speeds 10 % higher and magnetic fields 16 % higher than SIR-related ICMEs. This may imply that ICME-like transients represent events that occur closer to SIRs, and thus they are strongly compressed and their source regions are likely distributed

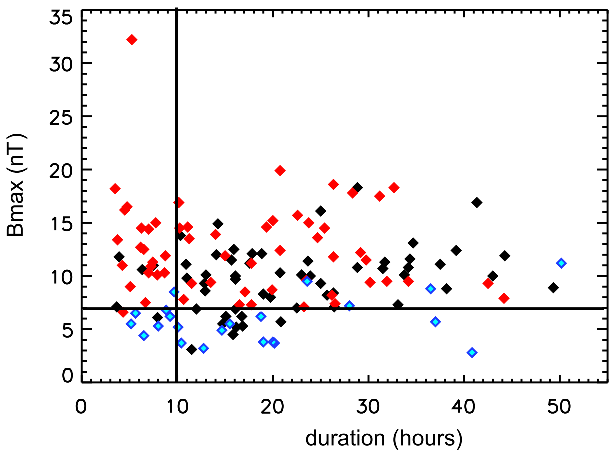

Figure 5 Scatter plot of maximum magnetic fields and durations for events: (black) embedded in the slow solar wind, (red) occurring close to or within SIRs, and (blue) embedded within declining parts of fast solar wind. Horizontal line indicates the magnetic field value of 7 nT and the vertical line duration of ten hours, the thresholds that were used to divide between the ICMEs and ICME-like transients.

Table 6 Maximum magnetic fields ($B_{\max}$), average speeds (V_{ave}), and durations (ΔT) for ICMEs and transients in three solar wind categories (see Section 2).

	$B_{\max}$ (nT)	V_{ave} (km s^{-1})	ΔT (h)
Category 1			
ICMEs	11.0	363.7	25.5
Transients	6.9	351.3	12.8
Category 2			
ICMEs	11.8	377.8	22.0
Transients	13.8	418.6	7.4
Category 3			
ICMEs	9.0	440.2	30.0
Transients	5.0	416.5	12.7

close to the western coronal hole boundaries. The majority (83 %) of events we identified within declining parts of fast solar wind were ICME-like transients. We suggest that these events arise from eastern boundaries of coronal holes and are ejected to rarefied solar wind streams. Such eruptions can easily expand, leading to low magnetic field magnitudes and long durations. Hence, our study suggests that ICME-like transients tend to originate close to coronal hole boundaries and they may play an important role in coronal hole dynamics (see, *e.g.*, Lionello *et al.*, 2005).

As discussed in the Introduction, solar observations suggest that interplanetary counterparts of weak coronal ejections would be observed on a daily basis. Our ICME-like transient rate was considerably smaller; on average less than one event per month was identified at each spacecraft. We emphasize that the identification of weak and small solar wind transients is subjective by its nature. It is highly possible that the majority of interplanetary counterparts of narrow CMEs and streamer blobs are merged as a part of the ambient solar wind while they travel from the Sun to the orbit of the Earth; thus their identification is extremely difficult, if not impossible. Future observations by ESA's *Solar Orbiter* and NASA's *Solar Probe Plus* will give new insight into the analysis of these structures, as these instruments allow one to study them much closer to the Sun than is currently possible. Our listing of

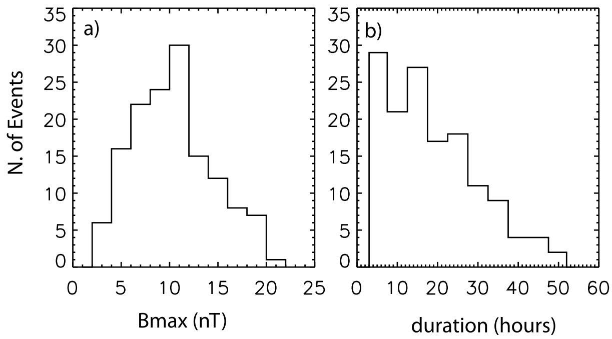

Figure 6 Distributions of (a) maximum magnetic field magnitudes and (b) durations for ICMEs and ICME-like transients. Magnetic field magnitudes are divided into 2 nT bins and durations into five hour bins.

small transients forms an important data base for efforts to connect remote coronagraph and heliospheric imager observations to *in situ* observations.

Acknowledgements We thank R.P. Lin for the *Wind* 3D plasma data and K.W. Ogilvie for the *Wind* SWE data. Support for the STEREO mission data processing and analysis was provided through NASA contracts to the IMPACT and PLASTIC teams (the IMPACT contract to University of California Berkeley NAS5-03131, and the PLASTIC contract to the University of New Hampshire NAS5-00132). STEREO supra-thermal electron pitch angle distributions were achieved through the CESR SWEA server. We thank Andrea Opitz for validating the STEREO pitch angle distributions and Peter Schroeder and Davin Larson for compiling the *Wind* pitch angle distributions. The LASCO CME catalogue is generated and maintained at the CDAW Data Center by NASA and The Catholic University of America in cooperation with the Naval Research Laboratory. SOHO is a project of international cooperation between ESA and NASA. STEREO magnetic field and plasma data were obtained through the UCLA Space Physics Center. The Academy of Finland project 130298 is thanked for its financial support.

References

Acuña, M.H., Curtis, D., Scheifele, J.L., Russell, C.T., Schroeder, P., Szabo, A., Luhmann, J.G.: 2008, The STEREO/IMPACT magnetic field experiment. *Space Sci. Rev.* **136**, 203 – 226.

Baker, D., Rouillard, A.P., van Driel-Gesztelyi, L., Démoulin, P., Harra, L.K., Lavraud, B., Davies, J.A., Opitz, A., Luhmann, J.G., Sauvaud, J.-A., Galvin, A.B.: 2009, Signatures of interchange reconnection: STEREO, ACE and *Hinode* observations combined. *Ann. Geophys.* **27**, 3883 – 3897.

Bothmer, V., Schwenn, R.: 1998, The structure and origin of magnetic clouds in the solar wind. *Ann. Geophys.* **16**, 1 – 24.

Burlaga, L., Plunkett, S.P., St. Cyr, O.C.: 2002, Successive CMEs and complex ejecta. *J. Geophys. Res.* **107**, 1266.

Burlaga, L., Sittler, E., Mariani, F., Schwenn, R.: 1981, Magnetic loop behind an interplanetary shock: Voyager, Helios and IMP 8 observations. *J. Geophys. Res.* **86**, 6673 – 6684.

Cartwright, M.L., Moldwin, M.B.: 2008, Comparison of small-scale flux rope magnetic properties to large-scale magnetic clouds: Evidence for reconnection across the HCS? *J. Geophys. Res.* **113**, A09105.

Feng, H.Q., Wu, D.J., Lin, C.C., Chao, J.K., Lee, L.C., Lyu, L.H.: 2008, Interplanetary small- and intermediate-sized magnetic flux ropes during 1995 – 2005. *J. Geophys. Res.* **113**, A12105.

Galvin, A.B., Kistler, L.M., Popecki, M.A., Farrugia, C.J., Simunac, K.D.C., Ellis, L., *et al.*: 2008, The plasma and suprathermal ion composition (PLASTIC) investigation on the STEREO observatories. *Space Sci. Rev.* **136**, 437 – 486.

Gilbert, H.R., Serex, E.C., Holzer, T.E., MacQueen, R.M., McIntosh, P.S.: 2001, Narrow coronal mass ejections. *Astrophys. J.* **550**, 1093 – 1101.

Gosling, J.T.: 1990, Coronal mass ejections and magnetic flux ropes in interplanetary space. In: Priest, E.R., Lee, L.C., Russell, C.T. (eds.) *Physics of Magnetic Flux Ropes, Geophys. Monogr.* **58**, 343 – 364.

Huttunen, K.E.J., Schwenn, R., Bothmer, V., Koskinen, H.E.J.: 2005, Properties and geoeffectiveness of magnetic clouds in the rising, maximum and early declining phases of solar cycle 23. *Ann. Geophys.* **23**, 625 – 641.

Jian, L., Russell, C.T., Luhmann, J.G.: 2011, Comparing solar minimum 23/24 with historical solar wind records at 1 AU. *Solar Phys.* **274**, 321 – 344. doi:10.1007/s11207-011-9737-2.

Jian, L., Russell, C.T., Luhmann, J.G., Skoug, R.M.: 2006, Properties of interplanetary coronal mass ejections at one AU during 1995 – 2004. *Solar Phys.* **239**, 393 – 436.

Kaiser, M., Kucera, T.A., Davila, J.M., St. Cyr, O.C., Guhathakurta, M., Christian, E.: 2008, The STEREO mission: An introduction. *Space Sci. Rev.* **136**, 5 – 16.

Kilpua, E.K.J., Luhmann, J.G., Gosling, J., Li, Y., Elliott, H., Russell, C.T., Jian, L., Galvin, A.B., Larson, D., Schroeder, P., Simunac, K., Petrie, G.: 2009a, Small solar wind transients and their connection to the large-scale coronal structure. *Solar Phys.* **256**, 327 – 344.

Kilpua, E.K.J., Pomoell, J., Vourlidas, A., Vainio, R., Luhmann, J., Li, Y., Schroeder, P., Galvin, A.B., Simunac, K.: 2009b, STEREO observations of interplanetary coronal mass ejections and prominence deflection during solar minimum period. *Ann. Geophys.* **27**, 4491 – 4503.

Kilpua, E.K.J., Liewer, P.C., Farrugia, C., Luhmann, J.G., Möstl, C., Li, Y., Liu, Y., Lynch, B., Russell, C.T., Vourlidas, A., Acuna, M.H., Galvin, A.B., Larson, D., Sauvaud, J.A.: 2009c, Multispacecraft observations of magnetic clouds and their solar origins May 19 – 23, 2007. *Solar Phys.* **254**, 325 – 344.

Kilpua, E.K.J., Jian, L.K., Li, Y., Luhmann, J.G., Russell, C.T.: 2011a, Multipoint ICME encounters: Pre-STEREO and STEREO observations. *J. Atmos. Solar-Terr. Phys.* **73**, 1228 – 1241.

Kilpua, E.K.J., Lee, C.O., Luhmann, J.G., Li, Y.: 2011b, Interplanetary coronal mass ejections in the near–Earth solar wind during the minimum periods following solar cycles 22 and 23. *Ann. Geophys.* **29**, 1455 – 1467.

Lavraud, B., Opitz, A., Gosling, J.T., Rouillard, A.P., Meziane, K., Sauvaud, J.-A., Fedorov, A., Dandouras, I., Genot, V., Jacquey, C., Louarn, P., Mazelle, C., Penou, E., Larson, D.E., Luhmann, J.G., Schroeder, P., Jian, L., Russell, C.T., Foullon, C., Skoug, R.M., Steinberg, J.T., Simunac, K.D., Galvin, A.B.: 2010, Statistics of counter-streaming solar wind suprathermal electrons at solar minimum: STEREO observations. *Ann. Geophys.* **28**, 233 – 246.

Lepping, R.P., Acuña, M.H., Burlaga, L.F., Farrell, W.M., Slavin, J.A., Schatten, K.H., Mariani, F., Ness, N.F., Neubauer, F.M., Whang, Y.C., Byrnes, J.B., Kennon, R.S., Panetta, P.V., Scheifele, J., Worley, E.M.: 1995, The *Wind* magnetic field investigation. *Space Sci. Rev.* **71**, 207 – 229.

Lepping, R.P., Berdichevsky, D.B., Wu, C.-C., Szabó, A., Narock, T., Mariani, F., Lazarus, A.J., Quivers, A.J.: 2006, A summary of WIND magnetic clouds for years 1995 – 2003: Model-fitted parameters, associated errors and classifications. *Ann. Geophys.* **24**, 215 – 245.

Li, Y., Luhmann, J.G., Lynch, B.J., Kilpua, E.K.J.: 2011, Cyclic reversal of magnetic cloud poloidal field. *Solar Phys.* **270**, 331 – 346.

Lin, R.P., Anderson, K.A., Ashford, S., Carlson, C., Curtis, D., Ergun, R., Larson, D., McFadden, J., McCarthy, M., Parks, G.K., Reme, H., Bosqued, J.M., Coutelier, J., Cotin, F., D'Uston, C., Wenzel, K.-P., Sanderson, T.R., Henrion, J., Ronnet, J.C., Paschmann, G.: 1995, A three-dimensional plasma and energetic particle investigation for the *Wind* spacecraft. *Space Sci. Rev.* **71**, 125 – 153.

Lionello, R., Riley, P., Linker, J.A., Mikic, Z.: 2005, The effects of differential rotation on the magnetic structure of the solar corona: Magnetohydrodynamic simulations. *Astrophys. J.* **625**, 463 – 473.

Malandraki, O., Saris, E.T., Kasotakis, Gr., Sidiropoulos, N.: 2000, Study of CME structure and evolution deduced from Ulysses/Hi-Scale energetic particle observations. *Adv. Space Res.* **26**, 875 – 878.

Moldwin, M.B., Ford, S., Lepping, R., Slavin, J., Szabo, A.: 2000, Small-scale magnetic flux ropes in the solar wind. *Geophys. Res. Lett.* **27**, 57 – 60.

Mulligan, T., Russell, C.T., Luhmann, J.G.: 1998, Solar cycle evolution of the structure of magnetic clouds in the inner heliosphere. *Geophys. Res. Lett.* **25**, 2959 – 2962.

Neugebauer, M., Goldstein, R.: 1997, Particle and field signatures of coronal mass ejections in the solar wind. In: Crooker, N., Joselyn, J.A., Feynman, J. (eds.) *Coronal Mass Ejections*, *Geophys. Monogr.* **99**, AGU, Washington, 245.

Richardson, I.G., Cane, H.V.: 1995, Regions of abnormally low proton temperature in the solar wind (1965 – 1991) and their association with ejecta. *J. Geophys. Res.* **100**, 23397.

Richardson, I.G., Cane, H.V.: 2010, Near-Earth interplanetary coronal mass ejections during solar cycle 23 (1996 – 2009): catalog and summary of properties. *Solar Phys.* **264**, 189 – 237.

Rouillard, A.P., Sheeley, N.R., Cooper, T., Davies, J.A., Lavraud, B., Kilpua, E.K.J., Skoug, R.M., Steinberg, J.T.: 2011, The solar origin of small interplanetary transients. *Astrophys. J.* **734**, 7. doi:10.1088/0004-637X/734/1/7.

Russell, C.T., Shinde, A.A., Jian, L.: 2005, A new parameter to define interplanetary coronal mass ejections. *Adv. Space Res.* **12**, 2178 – 2184.

Sauvaud, J.-A., Larson, D., Aoustin, C., Curtis, D., Medale, J.-L., Fedorov, A., Rouzaud, J., Luhmann, J., Moreau, T., Schröder, P., Louarn, P., Dandouras, I., Penou, E.: 2008, The IMPACT solar Wind electron analyzer (SWEA). *Space Sci. Rev.* **136**, 227 – 239.

Sheeley, N.R., Jr., Wang, Y.-M., Hawley, S.H., Brueckner, G.E., Dere, K.P., Howard, R.A., Koomen, M.J., Korendyke, C.M., Michels, D.J., Paswaters, S.E., Socker, D.G., St. Cyr, O.C., Wang, D., Lamy, P.L., Llebaria, A., Schwenn, R., Simnett, G.M., Plunkett, S., Biesecker, D.A.: 1997, Measurements of flow speeds in the corona between 2 and 30 R_{Sun}. *Astrophys. J.* **484**, 472 – 478.

Sheeley, N.R., Jr., Herbst, A.D., Palatchi, C.A., Wang, Y.-M., Howard, R.A., Moses, J.D., Vourlidas, A., Newmark, J.S., Socker, D.G., Plunkett, S.P., Korendyke, C.M., Burlaga, L.F., Davila, J.M., Thompson, W.T., St. Cyr, O.C., Harrison, R.A., Davis, C.J., Eyles, C.J., Halain, J.P., Wang, D., Rich, N.B., Battams, K., Esfandiari, E., Stenborg, G.: 2008, Heliospheric images of the solar wind at Earth. *Astrophys. J.* **675**, 853 – 862.

Sheeley, N.R., Jr., Lee, D.D.-H., Casto, K.P., Wang, Y.-M., Rich, N.B.: 2009, The structure of streamer blobs. *Astrophys. J.* **694**, 1471 – 1480.

Vourlidas, A., Howard, R.A., Esfandiari, E., Patsourakos, S., Yashiro, S., Michalek, G.: 2011, Erratum: Comprehensive analysis of coronal mass ejection mass and energy properties over a full solar cycle. *Astrophys. J.* **730**, 1.

Wang, Y.-M., Sheeley, N.R., Jr., Socker, D.G., Howard, R.A., Rich, N.B.: 2000, The dynamical nature of coronal streamers. *J. Geophys. Res.* **105**, 25133 – 25142.

Zurbuchen, T.H., Richardson, I.G.: 2006, *In-situ* solar wind and magnetic field signatures of interplanetary coronal mass ejections. *Space Sci. Rev.* **123**, 31 – 43.

Yashiro, S., Michalek, G., Gopalswamy, N.: 2008, A comparison of coronal mass ejections identified by manual and automatic methods. *Ann. Geophys.* **26**, 3103 – 3112.